Journal of Superconductivity and Novel Magnetism (2019) 32:3201–3209
https://doi.org/10.1007/s10948-019-5083-7

ORIGINAL PAPER

Determination of Phase Composition of Cobalt Nanoparticles Using ^{59}Co Internal Field Nuclear Magnetic Resonance

M. Manjunatha[1] · G. Srinivas Reddy[2] · K. J. Mallikarjunaiah[3] · Ramakrishna Damle[1] · K. P. Ramesh[4]

Received: 23 December 2018 / Accepted: 14 March 2019 / Published online: 29 March 2019

Abstract

It is well known that cobalt exhibits polymorphism, i.e., the co-existence of both the *hcp* and *fcc* phases. In particular, the method of synthesis and other thermodynamic conditions is known to play a crucial role in determining the particular phase of cobalt. In this work, we have compared the phase composition of the cobalt nanoparticles synthesized using two different solvents (water) and ethanol (Co@C). XRD measurements confirm the existence of *fcc* phase in commercial cobalt nanoparticles (Co@A), co-existence of *fcc* and *hcp* phases in Co@B, while the existence of the *hcp* phase in Co@C. We have studied these cobalt nanoparticles using ^{59}Co internal field nuclear magnetic resonance (IFNMR) for verification of phase composition. Our studies reveal that the Co@A has *fcc* as a major phase with minor quantity *hcp* phase. Co@B exhibits approximately equal amount of *fcc* and *hcp* phase while Co@C exhibits *hcp* as a major phase with minor *fcc* phase. Our SEM micrograph studies confirm that the cobalt particles have spherical shape in the *fcc* phase. The cobalt particles exhibit both spherical and dendrite morphology confirming the co-existence of *fcc* and *hcp* phases, while the sample with pure *hcp* phase exhibits the dendrite morphology. Our studies also throw light on understanding the effect of solvent in the phase formation of the cobalt nanoparticles.

Keywords ^{59}Co IFNMR · NMR line shape analysis · Cobalt nanoparticles · Solvent viscosity · Phase composition

1 Introduction

In recent years, ferromagnetic metallic (FM) nanoparticles have found potential applications in optical, magnetic, electronic, and catalytic materials [1, 2]. In practice, there are different approaches to synthesize the metallic nanoparticles. Depending on the kind of materials to be synthesized, various methods such as thermal decomposition [3], micro-emulsion technique [4], metal salt reduction [5], thermal and sonochemical reduction [6] have been employed. Method of synthesis is known to play a vital role in the formation of various phases of FM materials. The presence of various phases in materials is interesting and can be visualized through various available spectroscopic techniques. In the present study, we have taken up the study of cobalt system, which is ferromagnetic and exhibits polymorphism. It is well known that at normal conditions, bulk cobalt crystallizes in two phases: hexagonal closed packing (*hcp*) and face-centered cubic (*fcc*) [7]. The striking difference between these two phases is stacking of atoms, i.e., in *fcc*, it is ABCABC while in *hcp* cobalt, it is ABABAB [8]. Earlier studies on cobalt systems revealed that the synthesis conditions affect the phase formations and lead to either single or mixed phases. Hence, one has to consider three important parameters while synthesizing the cobalt particles by controlling (i) the synthesis temperature, (ii) chemical environment (solvents), and (iii) crystallite size of the cobalt particles [9]. It is found that a single exclusive phase formation is probable when low-temperature methods are employed, while the combination of phases is probable when high-temperature methods are adopted. Dinega et al. [10] have concluded that low activation energy for formation of the stacking faults is responsible for the

M. Manjunatha and G. Srinivas Reddy contributed equally to this work.

✉ K. P. Ramesh
kpramesh@iisc.ac.in

[1] Department of Physics, Bangalore University, Bengaluru 560056, India

[2] Undergraduate Program-Materials, Indian Institute of Science, Bengaluru 560012, India

[3] Undergraduate Program-Physics, Indian Institute of Science, Bengaluru 560012, India

[4] Department of Physics, Indian Institute of Science, Bengaluru 560012, India

existence of both the phases in the sample under high-temperature crystallization conditions, such as melting crystallization and evaporation condensation. Further, they also suggested that low-temperature solution chemistry methods yield exclusively single phase of cobalt [10]. O'Shea et al. [11] have reported that the stability of the phase of cobalt depends on the size of the particle, reduction atmosphere, and temperature. Kitakami et al. [9] have synthesized cobalt nanoparticles and found that depending on the particle size either it exists in *fcc* (less than 20 nm) or *hcp* (above 40 nm). Both the phases are preferred if the particle size is between 20 and 40 nm [9]. Cobalt powders synthesized via wet chemical route are generally not thermodynamically stable which enhances the possibility of formation of multiphase (*fcc* and *hcp*). In view of all these discussions, it appears that the synthesis of exclusive phases of cobalt is a bit cumbersome. In addition, to avoid the oxidation and agglomeration, nanoparticles must be capped during the reaction which can be achieved with the help of inert gases and the surfactants. Among different synthesis methods, metal salt reduction through co-precipitation process is faster, economical, and cleaner. In the present work, we have chosen an alternate synthesis method instead of the conventional methods which uses argon atmosphere or Teflon-lined stainless steel autoclave [12]. This modified synthesis method is discussed in the experimental section.

In this work, we have estimated the composition of different cobalt nanoparticles using ^{59}Co internal field nuclear magnetic resonance (IFNMR) technique and compared the results with the XRD measurements. Further structural and magnetic properties are determined using a scanning electron microscope (SEM) and vibrating sample magnetometry (VSM) techniques.

2 Experimental

2.1 Synthesis of the Sample

We have synthesized the Co metal nanopowders using co-precipitation method by designing a simple air exhausting device which avoids the requirement of an inert atmosphere. All the chemicals were of analytical grade and used for this preparation without further purification. In a typical synthesis [13], 1 g of $CoCl_2{\cdot}6H_2O$ dissolved in 50 ml of de-ionized water or ethanol at room temperature. Two milliliters of polyethylene glycol was added to the above solution as a surfactant. The solution was stirred using a magnetic stirrer to obtain a homogeneous solution. NaOH solution was prepared in another beaker by dissolving 5 g of NaOH pellets in 20 ml of de-ionized water. NaOH solution and 10 ml $N_2H_4{\cdot}H_2O$ were added step by step into the above precursor solution. This mixture was vigorously stirred and heated to 80 °C in a controlled setup. In order to avoid the air, the reaction was carried out in a flask having a side neck outlet which is connected to pipe immersed in water. The gases and vapors released during the reaction were bubbled into this beaker. The solution was maintained at the synthesis temperature for 45 min. The resulting black precipitate was filtered and washed with ethanol several times to remove the unreacted chloride ions and then dried in vacuum at 50 °C for 2 h. This method has yielded two samples for corresponding water and ethanol solvent. Further, we have also procured a commercial carbon-encapsulated cobalt sample (99.99% pure form, M/S Sigma-Aldrich) which is labeled as Co@A. The sample prepared with water as a solvent is labeled as Co@B and the other with ethanol is labeled as Co@C.

2.2 Characterization of the Samples

XRD is a powerful technique to elucidate the structure and phase of any materials. However, it may be difficult if the size of the particles is in nano range. Sometimes, XRD pattern analysis for cobalt has complications when the sample has both *fcc* and *hcp* phases co-existing, yield three and six peaks, respectively. However, the peaks observed at $2\theta = 44°$ and 76° of *fcc* and *hcp* almost overlap with each other leading to the ambiguous conclusion to arrive at the exact exclusive phase composition. Further, XRD peaks broaden and intensity diminishes, when the particle size reduces to nanometer scale or below, making them hard to observe. Hence, to circumvent these issues, we have relayed on IFNMR results which seems to throw light on phase identification and quantification [14].

IFNMR uses the internal field present at the nuclei for lifting the degeneracy of the energy levels. The condition for resonance in NMR is given by

$$f = \frac{\gamma H_{if}}{2\pi} \tag{1}$$

where γ is the gyromagnetic ratio of the given NMR nuclei (Hz/T), H_{if} is the hyperfine field experienced by the NMR active nuclei in tesla, f is the resonance frequency in MHz. There are only few IFNMR active nuclei (^{57}Fe, ^{59}Co, ^{61}Ni etc.,) with different gyromagnetic ratios and their corresponding NMR signals lie in the frequency range of ~ 20–750 MHz.

Specifically for cobalt, earlier reports revealed that in the *hcp* phase, the ^{59}Co nuclei experience slightly higher internal field (21.8 T) compared to that of *fcc*-phase (21.13 T) [15–17]. The gyromagnetic ratio of ^{59}Co is 10.102×10^6 Hz/T. Accordingly, one can expect different NMR signals corresponding to *hcp* (> 219 MHz) and *fcc* (> 212 MHz) phases of cobalt [14, 15, 18]. Typically, NMR signals of the two phases separated by ~ 7 MHz. Moreover, ^{59}Co being 100% abundant leads to detect and distinguish even the smallest contribution from each phase to the system.

In order to verify the phase purity of the cobalt sample and to authenticate our synthesis procedure, X-ray diffraction measurement has been carried out using an X' Pert PRO, PAN analytical diffractometer with Cu-K_α radiation (λ = 0.154 nm). Surface morphology of the synthesized particles is measured using field emission scanning electron microscopy (Zeiss make). The room temperature magnetic hysteresis loops of the powder samples were obtained (at ± 2 T) using a "Quantum design" Magnetic Property Measurement System (MPMS). ^{59}Co NMR of all the samples is studied using IFNMR spectrometer which is assembled in the lab and the details of the same can be found elsewhere [19]. NMR signals in all the samples have been observed using spin echo sequence ($\pi/2$-τ-π). We have used a $\pi/2$ pulse of width 1.0 μs and the delay between the two pulses is 20 μs. The $\pi/2$ pulse is optimized for the highest NMR spin-echo amplitude. The signals are recorded by measuring the spin echo amplitude as a function of frequency (in steps of 0.5 MHz) over the range 200–240 MHz. The quality factor Q of the probe circuit is maintained constant over the entire scanned range of frequencies.

3 Results and Discussions

3.1 XRD Measurements

XRD measurements of all the three samples are represented in Fig. 1. From the figure, one can notice that the sample Co@A has XRD peaks corresponding to only the *fcc*-phase (in agreement with the ICSD data), while the sample Co@B has XRD peaks corresponding to both *fcc* and *hcp* phases. On the other hand, Co@C has XRD peaks corresponding to only the *hcp* phase. One more striking observation in Co@B is that the XRD peak due to (200) plane corresponding to *fcc* phase reveals a slightly broadened and shift in the peak position compared to the pure phase which can be attributed to the presence of *hcp* stacking faults in the material which is in agreement with the similar observation of Andreev et al. [20]. The crystallite size (also known as coherent domain size) 'D' is calculated from the XRD using Debye-Scherer formula,

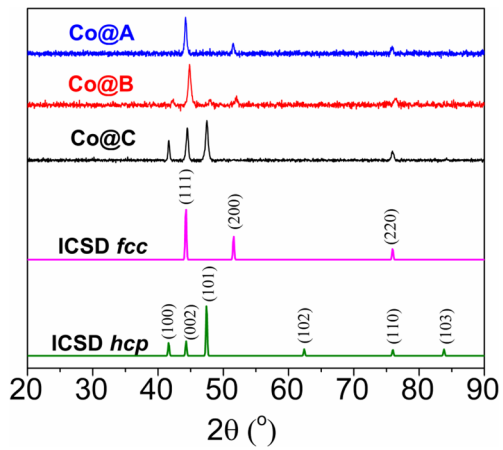

Fig. 1 The XRD patterns of the three different cobalt nanoparticles

$$D = \frac{0.9\lambda}{\beta \cos\theta} \tag{2}$$

where β is the full width of half maximum in (2θ), θ is the corresponding Bragg angle, $\lambda = 0.154$ nm. The crystallite sizes for the Co@A and Co@C samples are calculated with reference to the peak at angle at ~ 44°. The average crystallite sizes for Co@A and Co@C samples are found to be ~ 21 nm and ~ 35 nm, respectively. On the other hand, the crystallite size for Co@B sample having both the phases is calculated separately at the peaks ~ 42° and ~ 48° (*hcp* signature peaks) and 52° peak (*fcc* signature peak). These calculations show that average crystallite sizes for *hcp* phase in Co@B samples are found to be ~ 30 nm ~ 34 nm, respectively, while the average crystallite size for *fcc* phase is found to be ~ 26 nm.

The several crystallites of cobalt at a given annealing temperature will agglomerate to form particles of various sizes [21, 22]. Depending on the size of the particles, different phases will result according to the observation of Kitakami et al. [9]. SEM micrographs are used to estimate the particle size and the details of which are discussed in the next section. It should be noted that XRD technique is unable to quantify the presence of minor phases in all the three samples.

3.2 SEM Measurements

Figure 2a–c shows the surface morphology for Co@A, Co@B, and Co@C samples, respectively. Cobalt nanoparticles in Co@A agglomerate in the spherical structure. It is noteworthy that earlier reports also suggest that pure *fcc* cobalt nanoparticles exist in the spherical shape [23, 24]. The cobalt particles in Co@B sample exist mostly in the spherical shape along with the minor quantity of flower-shaped dendrites. Cobalt particles in Co@C sample appear as leaf-like dendrite shape. Similar morphology for *hcp* cobalt is reported by Zhu et al. [25]. Hence, it is important to consider the surface morphology as one of the parameters in the growth of the cobalt nanoparticles. Thus, qualitatively, one can observe the morphological changes in all three samples.

The particle size estimated for each micrograph is given on the right side of the each image. The estimated average particle size corresponding to Co@A is less than 30 nm, which can be attributed to *fcc* phase. On the other hand, the micrographs of Co@B and Co@C show the average size of particles to be in the range 30–60 nm and 40–100 nm, respectively, which may be attributed to mixed phase and the exclusive *hcp* phase.

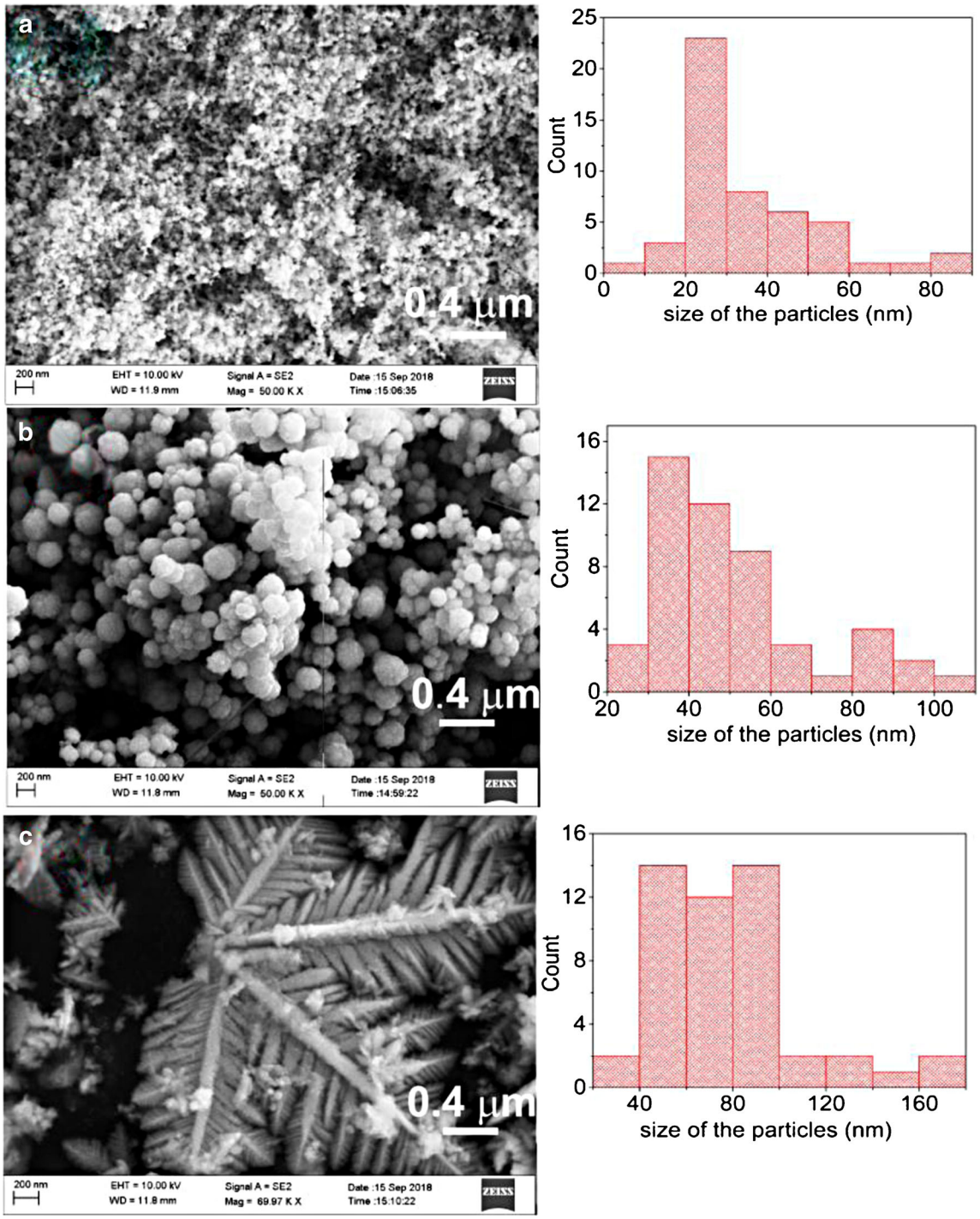

Fig. 2 SEM micrograph for all the three cobalt samples. Co@A consists of only spherical shape that contains major *fcc* phase. Co@B consists of both spherical shape and flower dendrite shape that coexists with almost equal amounts of *fcc* and *hcp* phases. Co@C which has leaf like dendrite consists of major *hcp* phase

XRD and SEM analysis leads to a conclusion that in Co@A, the coherent domain size is same as particle size. On the other hand, in Co@B, both small and larger particles are simultaneously co-exist, confirming the presence of smaller particles exhibiting single domain while the larger particles having multidomain particles. Co@C analysis also confirms the existence of single as well as agglomerated particles. A correlation between the particle size below which it exists in single domain (known as critical radius) and the corresponding magnetization is discussed in the next section.

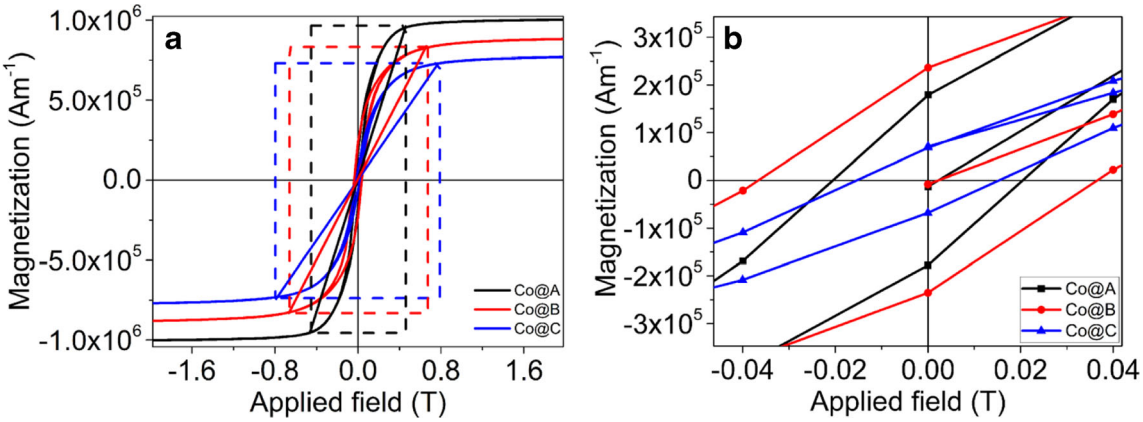

Fig. 3 **a** M versus H loops for the cobalt samples measured at RT. **b** Remanence and coercivity for the cobalt samples

3.3 Magnetic Measurements

Magnetic hysteresis loops for all the samples are shown in Fig. 3, which shows that the saturation magnetization (M_s) values for Co@A, Co@B, and Co@C samples are ~ 9.92 × 10^5 Am^{-1}, 8.44 × 10^5 Am^{-1}, and 7.46 × 10^5 Am^{-1}, respectively. The observed M_S values are used to calculate the critical radius (r_c) of the particles, below which they exist as the single domain particles, using the relation [26],

$$r_c = \frac{9\gamma}{\mu_0 M_S} \tag{3}$$

where γ is the domain wall energy of the cobalt (7.46 × 10^{-3} Jm^{-2}), μ_0 is the permeability of free space, and M_S is the saturation magnetization. The calculated r_c values are tabulated in Table 1. From the table, it is clear that the critical radius for the Co@A is smaller, while for Co@C, it is higher. The critical size estimated in the present study for the *fcc* phase is less than the previously reported values [27, 28], however much higher than the values estimated by the Kittel et al. [29]. The higher value of critical radius in our case is mainly due to the lower M_S values, compared to the M_S values of bulk cobalt particles (1.7 × 10^6 Am^{-1}) considered by Kittel et al. [29]. The coercive (H_c) and the remanence fields (H_r) are given in columns 4 and 5 of Table 1. The smaller values of H_c and H_r confirm the soft ferromagnetic nature of the cobalt nanoparticles. However, the H_c of Co@A (205 gauss) is higher than Co@C (158 gauss), which could be due to the presence of single domain particles.

The important factor in determining the phase of the cobalt is "anisotropy constant (K_a)", the dependence of magnetic properties on the direction of the applied field with respect to the crystal lattice [30, 31]. The anisotropy constant is calculated using the relation [26],

$$K_a = \frac{H_a \mu_0 M_S}{2} \tag{4}$$

where H_a is the anisotropy field obtained by extrapolating the M versus H graph for each sample as shown in Fig. 3. The calculated anisotropy constant is given in column 7 of Table 1. The estimated values of anisotropy constant for Co@A *(fcc)* and Co@C (*hcp)* phases are ~ 28 × 10^4 J/m^3 and ~ 39 × 10^4 J/m^3, respectively, which are in good agreement with the earlier reports [32, 33]. The anisotropy constant for the Co@B (*fcc* and *hcp*) is ~ 37 × 10^4 J/m^3. This variation of anisotropy constants is responsible for the various percentage of phase composition observed in the present cobalt nanoparticles.

3.4 Effect of Solvent and Temperature on the Phase Composition

It is well known from the literature that the chemical environment plays a very important role in obtaining the particular phase of the cobalt nanoparticles [9, 10, 23, 25]. Cobalt nanoparticles in the present studies were synthesized using a facile chemical route [13, 34]. Zhu et al. [25] have discussed the formation of cobalt nanoparticles with the help of following steps of chemical reactions,

Table 1 Parameters obtained from M versus H loop for the cobalt samples

Sample	Saturation magnetization (M_S) (Am^{-1}) × 10^5	Critical radius (r_c) (nm)	Coercive field (H_c) (T)	Remanence field (H_r) (Am^{-1}) × 10^5	Anisotropy field (H_a) (T)	Anisotropy constant (K_a) (Jm^{-3}) × 10^4
Co@A	9.92	55	0.0205	1.79	0.46	28
Co@B	8.44	73	0.0370	2.38	0.68	37
Co@C	7.46	99	0.0158	0.69	0.8	39

$$Co^{2+} + solvent \rightarrow Co(solvent)^{2+} \quad (5)$$

$$Co(solvent)^{2+} + mN_2H_4 \rightarrow Co(N_2H_4)_m^{2+} + n(solvent) \quad (6)$$

$$Co(N_2H_4)_m^{2+} + OH^- \rightarrow Co + N_2 + (m-1)N_2H_4 + H_2O \quad (7)$$

It is evident from the above equations that the solvent plays a significant role in the formation of the cobalt nanoparticles. Presence of hydrazine hydrate initiates the formation of the cobalt nanoparticles. The initial nucleating seeds will not have any specific preference for crystallographic phases; hence, simultaneous phases can be present. Further, the specific phase largely depends on the temperature. By tuning the synthesis temperature, the initial phase of the nucleating seeds can be monitored. After the initiation of the nucleation process, the growth mechanism can be controlled by the solvents [35] which selectively controls the surface energy of the different crystallographic phases [25]. Further, the viscosity of the solvent affects the reaction rate, the size, phase, and morphology of the cobalt nanoparticles. The high viscous solvents relatively hinder the formation spherical cobalt nanoparticles instead leads it to grow in a particular direction (anisotropic growth) leading to a formation of the leaf-like dendrite shape. On the other hand, a low viscous solvent offers less steric hindrance resulting in a growth of the cobalt particles. Moreover, the presence of surfactant minimizes the surface energy of the growth particle leading to a formation of the spherical particles.

It is well known that the *hcp* phase of bulk cobalt is more stable at low temperature (< 350 °C); however, the experimental results often show a mixture of *fcc* and *hcp* phase in nanoparticles prepared by chemical synthesis route. The low activation energy for the formation of stacking faults results in the formation of the mixed phase. Considering these facts, we have maintained the initial synthesis temperature at 80 °C. For Co@B, some cobalt ions are first reduced to cobalt atoms which further leads to the nucleation process. Remaining cobalt ions in the solutions help in the growth of particles. However, reaction speed is higher in water (less viscous 8.9×10^{-4} PaS) compared to ethanol leading to the formation of mixed phases [36, 37]. For Co@C, ethanol is used as a solvent. Due to its high viscosity (109.5×10^{-4} PaS), ethanol solvent allows the cobalt nanoparticles to unidirectional growth leading to a formation of the dendrite shape (2D growth). The high value of anisotropy observed for Co@C sample also supports this argument. The phase verification of these cobalt nanoparticles is done using ^{59}Co IFNMR studies which are discussed in the next section.

3.5 ^{59}Co IFNMR

Figure 4a–c shows the optimum NMR spectra of three different cobalt samples (Co@A, Co@B, and Co@C) measured at room temperature (RT). From Fig. 4, one can observe that there are

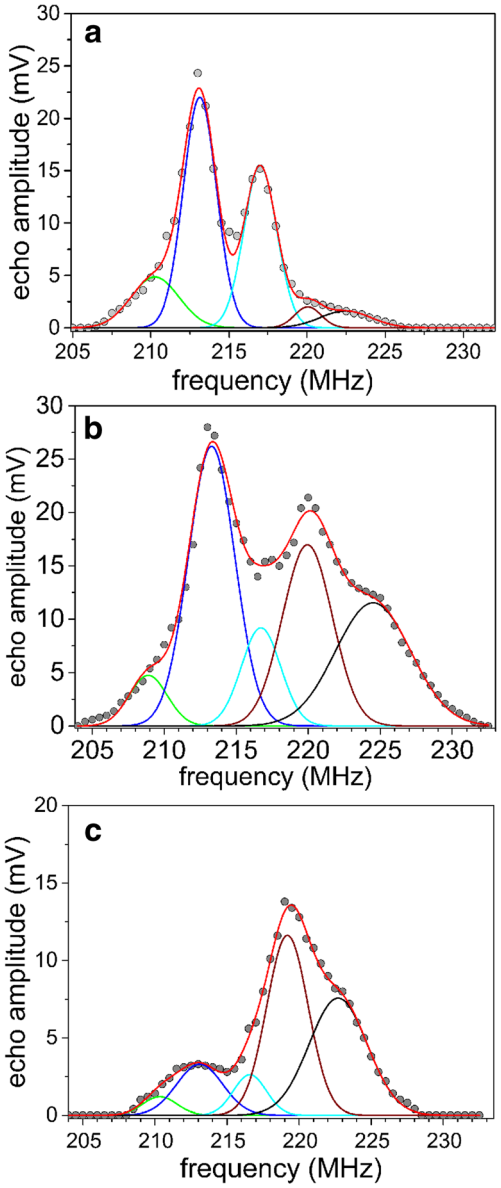

Fig. 4 ^{59}Co IFNMR spectra measured at room temperature for **a** Co@A (major *fcc* phase), **b** Co@B, **c** Co@C (major *hcp* phase). Each spectrum is deconvoluted to five sub-peaks as shown in the spectra. The black dot represents the experimental data, the green line represents the grain boundaries, blue line corresponds to the *fcc* domain wall, cyan corresponds to the *fcc* single domain, wine represents the *hcp* domain wall, and black line corresponds to the *hcp* single domain particles. Redline corresponds to the cumulative curve

two major peaks around ~ 213 and ~ 220 MHz, another three minor peaks ~ 210 MHz, ~ 217 MHz, and ~ 224 MHz. These peaks are deconvoluted using *Gaussian* fits and are assigned following the interpretation made in the earlier reports [13, 15, 35]. It is well known that ferromagnetic materials are bestowed with domains which are separated by the domain walls [29]. The behavior of the domain wall and domains are different for the applied radiofrequency (RF) field [38]. Based on the response of the domain wall and domains to RF, one can easily

distinguish their respective contributions to the total NMR signal amplitude. The applied RF field induces oscillations in the electronic moments of the ferromagnetic materials resulting in an RF component of the hyperfine field. Hence, one can expect an enhanced NMR signal both from domain and domain walls. However, the extent of RF enhancement is different for the domain (10^2 times) and domain wall (10^3 times) [38]; correspondingly, the induced NMR signal voltage at the probe is also different, leading to the variation in the intensities [39]. The response of the electronic moments (spins) for the applied RF in the domain walls is high as they are less pined than the electronic moments in the domains. Hence, for a given applied RF, the effective RF experienced by the domain wall is greater compared to the domains, which results in the higher NMR echo signal from domain walls compared to the domains. Due to this difference in the responses of the domains and domain walls, we have measured the NMR spectra at the optimum RF power levels (for maximum echo signal at a given NMR frequency). The variation of the RF power for optimum NMR signal as a function of frequency (in steps 0.5 MHz) is given in the Fig. 5. As discussed in the introduction, the internal field of the *fcc* and *hcp* domain walls is 21.10 T and 21.80 T, with the corresponding resonance frequencies are being ~ 213 MHz and ~220 MHz, respectively [15]. Hence, these signals are assigned to the *fcc* domain wall and *hcp* domain wall, respectively. Further, Gossard et al. have experimentally shown that the single domain cobalt nanoparticles resonate at ~ 217 MHz [40]. The higher value of this resonance frequency for single domain particles due to the addition of a demagnetizing field to the existing hyperfine field [27]. Similarly, the NMR signal observed around ~224 MHz was assigned to the *hcp* single domain particles. Sort et al. assigned the NMR signals observed between 205 and 210 MHz to the grain boundaries [41].

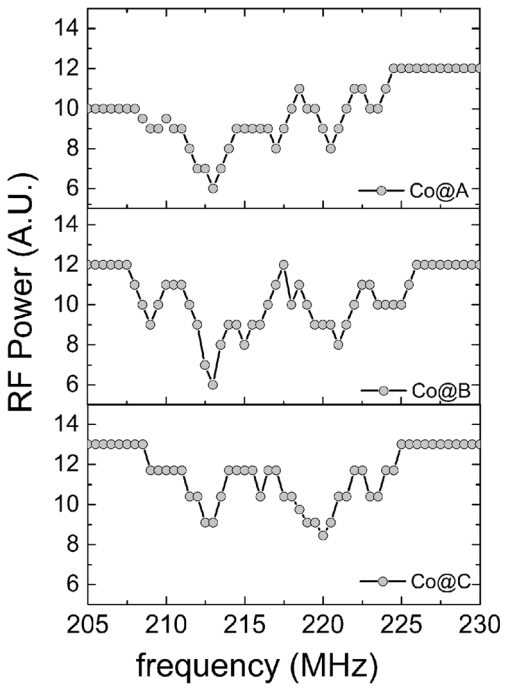

Fig. 5 Variation of RF power as a function of applied frequency for three different cobalt samples

Following the above discussions, we have assigned the deconvoluted NMR signals centered ~210 MHz to the grain boundaries and the peaks centered around 213 MHz and 217 MHz to *fcc* domain wall and the *fcc* single domain particles, respectively. Other two peaks centered around 220 MHz and 224 MHz were assigned to the *hcp* domain wall and the *hcp* single domain particles, respectively. Similar assignments of NMR peaks are also done for Co@B and Co@C. The area under each curve assigned above is calculated and tabulated in Table 2 for all the three samples. From the table, one can notice that all the three samples have different line shapes, indicating the contribution from different phases from their domain wall, domains, and grain boundaries. Further, it is also observed that the area under the peaks and their sum in each spectrum represent the percentage of each phase present in the individual sample.

From the Table 2, it is apparent that Co@A has ~80% *fcc* phase, ~8% of *hcp* phase, and remaining contribution from grain boundaries. Similarly, Co@B has ~50% of the *hcp* phase, ~43% of the *fcc* phase, and the remaining contribution from the grain boundaries. Finally, Co@C has ~77% of the *hcp* phase, ~20% of the *fcc* phase, and the remaining contribution from the grain boundaries. Thus, from ^{59}Co IFNMR studies, we can conclude that sample prepared using water (Co@B) as a solvent has almost equal percentage of both the phases, while the sample prepared using ethanol (Co@B) as a solvent has a major amount of *hcp* phase (~ 77%) and ~20% of *fcc* phase. Commercial cobalt (Co@C) sample prepared using the decomposition of cobalt carbonyl (mentioned by the manufacturer) contains ~80% of the *fcc* phase. Thus, ^{59}Co IFNMR line shape analysis represents a quantitative estimation of the percentage of phase composition in any ferromagnetic samples containing abundant NMR active nuclei.

3.6 Compositional Analysis: a Comparison Between NMR and XRD

The deconvoluted components from the NMR line shape show that *fcc* is a major phase in the Co@A, whereas Co@B has an equal contribution from the *fcc* and *hcp* phase. The Co@C has the majority of the *hcp* phase. As mentioned earlier, IFNMR technique is based on the local hyperfine field experienced by the NMR active nuclei (cobalt). The high value of the gyromagnetic ratio of the nuclei (~ 10.09×10^6 Hz/T) and its abundance (100%) makes it more sensitive technique in determining the phase composition. Moreover, the experimentally observed difference between *fcc* and *hcp* phases (Δf = 7 MHz) supports the better resolution of the

Table 2 Contribution to NMR signals from the different phase components measured at room temperature. The standard error in the decomposition of the NMR spectra is <± 5%

	Sample a		Sample b		Sample c	
Peak assignment	Frequency (MHz)	Area %	Frequency (MHz)	Area %	Frequency (MHz)	Area %
Grain boundaries	210.0	12.30	209.4	07.50	210.3	03.40
fcc domain wall	213.0	46.89	213.4	32.30	213.1	12.64
fcc single domain	217.0	33.23	216.7	10.28	216.6	07.14
hcp domain wall	220.7	04.89	220.0	24.68	219.2	40.21
hcp single domain	223.4	02.69	224.5	25.24	222.7	36.61

NMR technique. In the present work, the frequency scan is carried out in steps of 0.5 MHz with an RF pulse width of 1 μs. This implies that the bandwidth covered in each set frequency is ~ 1 MHz. Thus, a clear resolution between the two phases is evident. But still, we observe a minute contribution to the NMR signal from the *fcc* phase in *hcp* and vice versa which establishes the percentage of mixed phases which have helped us in estimating the percentage contribution of various phases. At this juncture, it should be noted that the XRD technique is not sensitive for such a small contribution. In view of the above arguments, the existence of the lower component of *hcp* in sample Co@A and *fcc* in sample Co@C is revealed by NMR but not observed in XRD. It is well known that at high frequencies, a higher population difference is maintained in accordance with the following equation,

$$\frac{N_-}{N_+} = \mathrm{e}^{-\frac{\gamma H_{if}}{KT}} \tag{8}$$

where N_+ is the number of spins in the lower levels and N_- is the number of spins present in the higher level, γ is the gyromagnetic ratio of the NMR active nuclei in Hz/T, H_{if} is the hyperfine field/applied field, K is the Boltzmann constant in J/K, and T is the temperature in K. This further enhances the sensitivity of NMR technique over XRD. Hence, a comparison of NMR line shape analysis with XRD results shows that the latter gives a qualitative presence of the various phases, while NMR gives the quantitative estimation of the phase composition with a better accuracy, which serves as a complimentary technique for NMR active magnetic materials.

Furthermore, from the present results, one can also conclude that it is impossible to synthesize an exclusive single phase of the cobalt nanoparticles. However, one can tune the phase composition using different synthesis techniques.

4 Conclusions

In the present work, we have synthesized the cobalt nanoparticles via co-precipitation method using two different solvents water (Co@B) and ethanol (Co@C). The XRD measurements show that Co@A (commercially procured carbon-encapsulated cobalt nanopowder) exists in *fcc* cobalt phase. Co@B shows the existence of both *fcc* and *hcp* phases, while the Co@C exhibit only the *hcp* phase. The SEM morphology studies for Co@A show the presence of spherical particles, while the Co@B shows the presence of both spherical and flower dendrite shape. The sample prepared using ethanol as solvent exhibits only the leaf-like dendrite shape. ^{59}Co IFNMR studies confirm that the existence of major phase in Co@A is *fcc*, co-existence of both *fcc* and *hcp* in Co@B and existence of major *hcp* phase in Co@C. From these analyses, we conclude that the final phase composition of the cobalt largely depends on the synthesis conditions like chemical environment, solvents, temperature etc., which alters the size and surface morphology of the cobalt particles. The high viscous solvent like ethanol favors the formation unidirectional growth (dendrite shape) of the particles leading to *hcp* phase of the cobalt and the low viscous solvents result in the rapid growth of spherical cobalt nanoparticles resulting in the formation of both *fcc* and *hcp* phase.

Acknowledgements The authors would like to thank Prof. A Sundareshan for the kind help in VSM measurements.

Compliance with Ethical Standards

Conflict of Interest The authors declare that they have no conflict of interest.

References

1. Lu, A.-H., Salabas, E.L., Schüth, F.: Magnetic nanoparticles: synthesis, protection, functionalization, and application. Angew. Chem. **46**, 1222–1244 (2007)
2. Michalek, F., Lagunas, A., Jimeno, C., Pericas, M.A.: Synthesis of functional cobalt nanoparticles for catalytic applications. Use in asymmetric transfer hydrogenation of ketones. J. Mater. Chem. **18**, 4692–4697 (2008)
3. Salavati-Niasari, M., Davar, F., Mazaheri, M., Shaterian, M.: Preparation of cobalt nanoparticles from [bis (salicylidene) cobalt

(II)]–oleylamine complex by thermal decomposition. J. Magn. Magn. Mater. **320**, 575–578 (2008)
4. Kumbhar, A., Spinu, L., Agnoli, F., Wang, K., Zhou, W.L., O'Connor, C.J.: Magnetic properties of cobalt and cobalt-platinum alloy nanoparticles synthesized via microemulsion technique. IEEE Trans. Magn. **37**, 2216–2218 (2001)
5. Sun, C., Murray, C.B.: Synthesis of monodisperse cobalt nanocrystals and their assembly into magnetic superlattices. J. Appl. Phys. **85**, 4325–4330 (1999)
6. Sun, Y.P., Rollins, H.W., Guduru, R.: Preparations of nickel, cobalt, and iron nanoparticles through the rapid expansion of supercritical fluid solutions (RESS) and chemical reduction. Chem. Mater. **11**, 7–9 (1999)
7. Jeon, Y.T., Moon, J.Y., Lee, G.H., Park, J., Chang, Y.: Comparison of the magnetic properties of metastable hexagonal close-packed Ni nanoparticles with those of the stable face-centered cubic Ni nanoparticles. J. Phys. Chem. B. **110**, 1187–1191 (2006)
8. Kajiwara, S., Ohno, S., Honma, K., Uda, M.: A new crystal structure of pure cobalt formed in ultrafine particles. Philos. Mag. Lett. **55**, 215–219 (1987)
9. Kitakami, O., Sato, H., Shimada, Y., Sato, F., Tanaka, M.: Size effect on the crystal phase of cobalt fine particles. Phys. Rev. B. **56**, 13849 (1997)
10. Dinega, D.P., Bawendi, M.: A solution-phase chemical approach to a new crystal structure of cobalt. Angew. Chem. **38**, 1788–1791 (1999)
11. Pena O'Shea, V.A., Piscina, P.R., Homs, N., Aromí, G., Fierro, J.L.G.: Development of hexagonal closed-packed cobalt nanoparticles stable at high temperature. Chem. Mater. **21**, 5637–5643 (2009)
12. Niu, H., Chen, Q., Zhu, H., Lin, Y., Zhang, X.: Magnetic field-induced growth and self-assembly of cobalt nanocrystallites. J. Mater. Chem. **13**, 1803–1805 (2003)
13. Mourdikoudis, S., Collière, V., Fau, P., Kahn, M.L.: A study on the synthesis of Ni_{50} Co_{50} alloy nanostructures with tuned morphology through metal–organic chemical routes. Dalton Trans. **43**, 8469–8479 (2014)
14. Choudhary, H.K., Manjunatha, M., Damle, R., Ramesh, K.P., Sahoo, B.: Solvent dependent morphology and ^{59}Co internal field NMR study of co-aggregates synthesized by wet chemical method. Phys. Chem. Chem. Phys. **20**, 17739–17750 (2018)
15. Kawakami, M., Hihara, T., Kōi, Y., Wakiyama, T.: The ^{59}Co nuclear magnetic resonance in hexagonal cobalt. J. Phys. Soc. Jpn. **33**, 1591–1598 (1972)
16. Andreev, A., Lapina, O., Cherepanova, S.: A new insight into cobalt metal powder internal field ^{59}Co NMR spectra. Appl. Magn. Reson. **45**, 1009–1017 (2014)
17. Shmyreva, A.A.: NMR investigation of metal nanoparticles by the example of ^{59}Co nanoparticles. Izd-vo Solo Press (Russian Federation). 44 105–109 (2013)
18. Manjunatha, M., Kumar, R., Siddesh, B.M., Sahoo, B., Damle, R., Ramesh, K.P.: Structural variation study of cobalt nanoparticles synthesized by co-precipitation method using ^{59}Co NMR. AIP. Conf. Proc. **1942**, 050115 (2018)
19. Siddesh, B.M., Manjunatha, M., Damle, R., Ramesh, K.P.: Fabrication of low cost and versatile internal field pulsed nuclear magnetic resonance spectrometer to study the magnetic materials. Indian J. Pure Appl. Phys. **56**, 859–868 (2018)
20. Andreev, A.S., d'Espinose de Lacaillerie, J.-B., Lapina, O.B., Gerashenko, A.: Thermal stability and hcp–fcc allotropic transformation in supported Co metal catalysts probed near operando by ferromagnetic NMR. Phys. Chem. Chem. Phys. **17**, 14598–14604 (2015)
21. Andreev, A.S., Kazakova, M.A., Ishchenko, A.V., Selyutin, A.G., Lapina, O.B., Kuznetsov, V.L., d'Espinose de Lacaillerie, J.-B.: Magnetic and dielectric properties of carbon nanotubes with embedded cobalt nanoparticles. Carbon. **114**, 39–49 (2017)
22. Kazakova, M.A., Andreev, A.S., Selyutin, A.G., Ishchenko, A.V., Shuvaev, A.V., Kuznetsov, V.L., Lapina, O.B., d'Espinose de Lacaillerie, J.-B.: Co metal nanoparticles deposition inside or outside multi-walled carbon nanotubes via facile support pretreatment. Appl. Surf. Sci. **456**, 657–665 (2018)
23. Li, H., Li, Y., Zhang, Y., Liang, C., Wang, H., Li, B., Adair, D., Bakenov, Z.: Fabrication and properties of carbon-encapsulated cobalt nanoparticles over NaCl by CVD. Nanoscale Res. Lett. **11**, 432 (2016)
24. Grass, R.N., Stark, W.J.: Gas phase synthesis of fcc-cobalt nanoparticles. J. Mater. Chem. **16**, 1825–1830 (2006)
25. Zhu, Y., Zheng, H., Yang, Q., Pan, A., Yang, Z., Qian, Y.: Growth of dendritic cobalt nanocrystals at room temperature. J. Cryst. Growth. **260**, 427–434 (2004)
26. Jiles, D.: Introduction to Magnetism and Magnetic Materials. CRC press, Boca Roten (2015)
27. Zhang, Y.D., Budnick, J.I., Hines, W.A., Majetich, S.A., Kirkpatrick, E.M.: Microstructure and magnetic behavior of carbon-coated Co nanoparticles studied by nuclear magnetic resonance. Appl. Phys. Lett. **76**, 94–96 (2000)
28. Leslie-Pelecky, D.L., Rieke, R.D.: Magnetic properties of nanostructured materials. Chem. Mater. **8**, 1770–1783 (1996)
29. Kittel, C.: Physical theory of ferromagnetic domains. Rev. Mod. Phys. **21**, 541 (1949)
30. Kittel, C.: On the theory of ferromagnetic resonance absorption. Phys. Rev. **73**, 155 (1948)
31. Kittel, C., McEuen, P.: Introduction to Solid State Physics. Wiley, New York (1996)
32. Chen, J., Sorensen, C., Klabunde, K., Hadjipanayis, G.: Magnetic properties of nanophase cobalt particles synthesized in inversed micelles. J. Appl. Phys. **76**, 6316–6318 (1994)
33. Meziane, L., Salzemann, C., Aubert, C., Gérard, H., Petit, C., Petit, M.: Hcp cobalt nanocrystals with high magnetic anisotropy prepared by easy one-pot synthesis. Nanoscale. **8**, 18640–18645 (2016)
34. Gu, H., Zheng, R., Zhang, X., Xu, B.: Facile one-pot synthesis of bifunctional heterodimers of nanoparticles: a conjugate of quantum dot and magnetic nanoparticles. J. Am. Chem. Soc. **126**, 5664–5665 (2004)
35. Wu, K.-L., Wei, X.-W., Zhou, X.-M., Wu, D.-H., Liu, X.-W., Ye, Y., Wang, Q.: $NiCo_2$ alloys: controllable synthesis, magnetic properties, and catalytic applications in reduction of 4-nitrophenol. J. Phys. Chem. C. **115**, 16268–16274 (2011)
36. Liu, X.-M., Gao, W.-L., Miao, S.-B., Ji, B.-M.: Versatile fabrication of dendritic cobalt microstructures using CTAB in high alkali media. J. Phys. Chem. Solids. **69**, 2665–2669 (2008)
37. Xia, X., Zeng, J., Oetjen, L.K., Li, Q., Xia, Y.: Quantitative analysis of the role played by poly (vinylpyrrolidone) in seed-mediated growth of Ag nanocrystals. J. Am. Chem. Soc. **134**, 1793–1801 (2012)
38. Wurmehl, S., Kohlhepp, J.T.: Nuclear magnetic resonance studies of materials for spintronic applications. J. Phys. D. **41**, 173002 (2008)
39. Liu, Y., Luo, J., Shin, Y., Moldovan, S., Ersen, O., Hébraud, A., Schlatter, G., Pham-Huu, C., Meny, C.: Sampling the structure and chemical order in assemblies of ferromagnetic nanoparticles by nuclear magnetic resonance. Nat. Commun. **7**, 11532 (2016)
40. Gossard, A., Portis, A., Rubinstein, M., Lindquist, R.: Ferromagnetic nuclear resonance of single-domain cobalt particles. Phys. Rev. **138**, A1415 (1965)
41. Sort, J., Surinach, S., Munoz, J., Baró, M., Wojcik, M., Jedryka, E., Nadolski, S., Sheludko, N., Nogués, J.: Role of stacking faults in the structural and magnetic properties of ball-milled cobalt. Phys. Rev. B. **68**, 014421 (2003)